

## Article

# Decarboxylation of *p*-Coumaric Acid during Pyrolysis on the Nanoceria Surface

Nataliia Nastasiienko <sup>1,\*</sup>, Tetiana Kulik <sup>1,\*</sup>, Borys Palianytsia <sup>1</sup>, Mats Larsson <sup>2</sup>, Tetiana Cherniavska <sup>1</sup>  
and Mykola Kartel <sup>1</sup>

<sup>1</sup> Chuiko Institute of Surface Chemistry, NAS of Ukraine, 17 General Naumov Str., 03164 Kyiv, Ukraine; borbor@i.ua (B.P.); t-cherniavska@ukr.net (T.C.); nikar@kartel.kiev.ua (M.K.)

<sup>2</sup> Department of Physics, AlbaNova University Center, Stockholm University, SE-106 91 Stockholm, Sweden; ml@fysik.su.se

\* Correspondence: nastasiienkon@ukr.net (N.N.); tanyakulyk.isc.ms@gmail.com (T.K.);  
Tel.: +38-044-422-9676 (N.N. & T.K.)

**Abstract:** Temperature-programmed desorption mass spectrometry (TPD MS) was used to study the pyrolysis of *p*-coumaric acid (*p*CmA) on the nanoceria surface. The interaction of *p*CmA with the CeO<sub>2</sub> surface was investigated by FT-IR spectroscopy. The obtained data indicated the formation on the nanoceria surface of bidentate carboxylate complexes with chelate ( $\Delta\nu = 62 \text{ cm}^{-1}$ ) and bridge structure ( $\Delta\nu = 146 \text{ cm}^{-1}$ ). The thermal decomposition of *p*CmA over nanoceria occurred in several stages, mainly by decarboxylation. The main decomposition product is 4-vinylphenol ( $m/z$  120). The obtained data can be useful for studying the mechanisms of catalytic thermal transformations of lignin-containing raw materials using catalysts containing cerium oxide and the development of effective technologies for the isolation of *p*CmA from lignin.

**Keywords:** temperature-programmed desorption mass spectrometry; FT-IR spectroscopy; 4-vinyl phenol; lignin; biomass conversion



**Citation:** Nastasiienko, N.; Kulik, T.; Palianytsia, B.; Larsson, M.; Cherniavska, T.; Kartel, M. Decarboxylation of *p*-Coumaric Acid during Pyrolysis on the Nanoceria Surface. *Colloids Interfaces* **2021**, *5*, 48. <https://doi.org/10.3390/colloids5040048>

Academic Editor: habil.  
Reinhard Miller

Received: 16 October 2021  
Accepted: 8 November 2021  
Published: 11 November 2021

**Publisher's Note:** MDPI stays neutral with regard to jurisdictional claims in published maps and institutional affiliations.



**Copyright:** © 2021 by the authors. Licensee MDPI, Basel, Switzerland. This article is an open access article distributed under the terms and conditions of the Creative Commons Attribution (CC BY) license (<https://creativecommons.org/licenses/by/4.0/>).

## 1. Introduction

*p*-Coumaric acid belongs to the class of hydroxycinnamic acids and is a biologically active compound of natural origin [1,2]. Free and bound *p*CmA is widely distributed in fruits, vegetables, and cereals [2]. *p*CmA is found in large quantities in lignin [3,4], ubiquitous in herbal lignin [4]. *p*CmA residues are attached to the main lignin macromolecule via ether bonds [5–8]. Lignin is a complex natural polymer; the monomeric units of which are *p*-coumaryl, coniferyl, and sinapyl alcohols linked by different types of C–O bonds [9]. Together with other components of lignocellulose (hemicellulose, cellulose), it is considered a potentially important source of valuable chemicals (biofuels, polymers, etc.). In particular, it can serve as a source of a wide range of aromatic compounds [10]. It is known that the pyrolysis of coumaric acid leads to the formation of 4-vinylphenol [11]. The presence of *p*CmA and other hydroxycinnamates in the plant biomass encourages the search for new cost-effective technologies to extract this acid from lignin and the selection of new herbaceous species enriched with this biologically active compound [4].

The development of such technologies is due to the need for a more efficient use of plant materials processed on biorefineries. It also speeds up the transition from fossil resources to more accessible, environmentally friendly, and renewable ones. The current wealth of genetic resources makes it possible to upregulate and downregulate the production of hydroxycinnamates with relative ease and to engineer plants that produce only *p*CmA [4]. Pyrolysis is one of the most promising methods for the conversion of lignocellulosic biomass [5]. Pyrolysis Mass Spectrometry is actively used in the quantitative analysis of *p*CmA in lignin-containing raw materials [7,8,12–14].

The use of catalysts is one way to achieve a more selective analysis, as well as biomass conversion [5]. Cerium dioxide, due to its catalytic properties [15], can be used both for

processing lignin products [16–18] and in the conversion of lignocellulosic raw materials [19,20]. However, its potential in this area is still insufficiently disclosed. Metal oxide catalysts CeO<sub>2</sub>/MexO<sub>y</sub> (Me = Si, Al, Zr, etc.), with an active phase deposited on a substrate, resulted in especially effective catalytic systems [21–23]. The acid-base surface properties of the support lead to a synergistic effect due to the interaction of the active phase with the support and, as a result, to an increase in the catalytic activity of such systems [21–26].

In our work, we studied *p*CmA complexes on the CeO<sub>2</sub> surface and their thermal transformations using TPD MS, FT-IR spectroscopy and thermogravimetric analysis. The results of this work can be helpful for the development of new technologies for the isolation of coumaric acid, as well as the pyrolytic processing of lignin using CeO<sub>2</sub>-based catalysts. This result can be useful for the development of pyrolytic methods for obtaining renewable 4-vinylphenol as a monomer block for new types of polymeric materials based on poly-(4-hydroxystyrene) [27,28].

## 2. Materials and Methods

Nanosized cerium dioxide (99.5%,  $S_{Ar} = 71 \text{ m}^2/\text{g}$ .) and *p*CmA ( $\geq 98\%$ ) were purchased from (Alfa Aesar, Karlsruhe, Germany). No further purification of these compounds was conducted in this work. CeO<sub>2</sub> was pre-calcined at 500 °C for 2 h to remove organic matter.

A series of samples *p*CmA/CeO<sub>2</sub> with *p*CmA concentrations in 0.1, 0.3, 0.6, 0.9, and 1.2 mmol/g were prepared (Table 1). The concentration range of 0.1–1.2 mmol/g was selected based on previous studies [29]. According to [29], the maximum adsorption values for cinnamic acids were almost equal and amounted to  $\approx 2.9 \times 10^{-4} \text{ mol/g}$ , irrespective of the differences in the reaction sites of their molecules. The samples were prepared by impregnating CeO<sub>2</sub> (100 mg) with *p*CmA ethanolic solution (2 mL). The suspensions were stirred for several minutes and then dried at room temperature in the air.

**Table 1.** The composition of the studied samples.

Sample	The Content of <i>p</i> -Coumaric Acid (mmol/g)
<i>p</i> CmA/CeO <sub>2</sub>	0.1
	0.3
	0.6
	0.9
	1.2

Infrared spectra were obtained on a Thermo Nicolet Nexus FT-IR instrument (ThermoNicolet Corporation, Madison, WI, USA) in the range 4000–400 cm<sup>-1</sup>, operating in the diffuse reflection mode. The resolution was 4 cm<sup>-1</sup>, and the number of scans was 50. For FT-IR studies, pure CeO<sub>2</sub> and *p*CmA/CeO<sub>2</sub> samples were mixed with KBr (1:10). Pure *p*CmA was mixed with KBr (1:100).

Thermal transformations of coumaric acid over nanoceria were studied using temperature-programmed desorption mass spectrometry on an MX-7304A monopole mass spectrometer (Electron, Sumy, Ukraine) with electron ionization, as described previously [30–34]. A sample weighing 10–20 mg was placed in a quartz-molybdenum ampoule and pumped out to a pressure of  $5.5 \times 10^{-4} \text{ Pa}$ , after which it was heated at a rate of 0.17 °C/s from 20 to 750 °C. The range of the studied masses was  $m/z$  1–210.

Thermogravimetric analysis was performed using a TGA/DTA analyzer (Q-1500D, Budapest, Hungary). Samples weighing 100 mg were heated from room temperature to 1000 °C. The heating rate was 10 °C/min in the air.

## 3. Results and Discussion

### 3.1. Fourier Transform–Infrared (FT–IR) Spectroscopy

The results of the FT-IR spectroscopic studies of *p*CmA/CeO<sub>2</sub> samples (0.1–1.2 mmol/g) are presented in Figure 1.

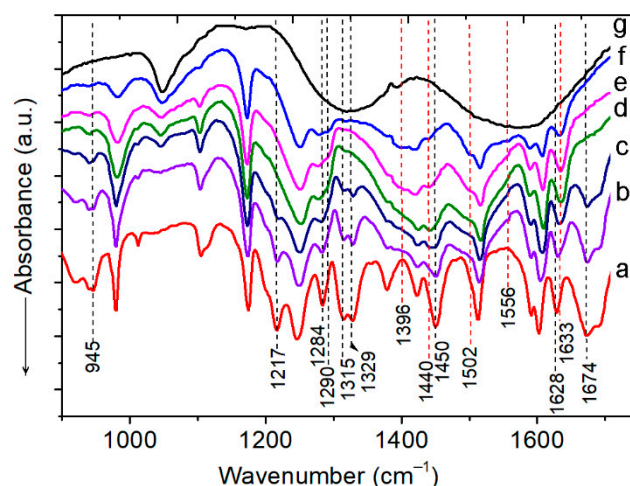


**Figure 1.** Fourier transform-infrared (FT-IR) spectra of pure *pCmA* (a), samples of *pCmA/CeO<sub>2</sub>* with different contents of *pCmA* (1.2: b, 0.9: c, 0.6: d, 0.3: e, and 0.1 mmol/g: f) and pure *CeO<sub>2</sub>* (g).

The main absorption bands (Table 2) were assigned based on the literature data [16,34–38]. The symbol “ $\nu$ ” denotes stretching vibrations, “ $\beta$ ” denotes in-plane deformations, and “ $\delta$ ” denotes out-of-plane deformations; the band is marked with “as”—asymmetric vibrations, “s”—symmetric, and “ar”—vibrations of the aromatic ring.

**Table 2.** Assignments of characteristic infrared bands of pure *pCmA* and of *pCmA/CeO<sub>2</sub>* (0.6 mmol/g).

Assignments	Frequency (cm <sup>-1</sup> )	
	<i>pCmA</i>	<i>pCmA/CeO<sub>2</sub></i>
$\delta(\text{COH})$	945	–
$\nu(\text{C-O})_{\text{ar}}$	1284	1279, 1290
$\nu(\text{CC})_{\text{ar}}$	1450	–
$\nu(\text{COO}^-)_{\text{s}}$	–	1396–1410
$\nu(\text{COO}^-)_{\text{s}}$	–	1440
$\nu(\text{CC})_{\text{ar}}$	1514	1516
$\nu(\text{COO}^-)_{\text{as}}$	–	1502
$\nu(\text{COO}^-)_{\text{as}}$	–	1556
$\nu(\text{CC})_{\text{ar}}$	1603	1608
$\nu(\text{C=C})$	1628	1633
$\nu(\text{C=O})$	1674	–
$\nu(\text{C=O})$	–	1684

Figure 1 showed that for samples of *pCmA/CeO<sub>2</sub>* (0.1–0.3 mmol/g) there was no band of carboxyl groups at 1674 ( $\nu(\text{C=O})$ ) [35] and band of 945 cm<sup>-1</sup>, where vibrations ( $\delta(\text{OH})$ ) were usually observed for carboxylic acids [34]. At the same time, carboxylate bands appeared at 1396 ( $\nu(\text{CO})$ ), 1410, 1440 cm<sup>-1</sup> ( $\nu_{\text{s}}(\text{COO}^-)$ ), and about 1502 and 1556 cm<sup>-1</sup> ( $\nu_{\text{as}}(\text{COO}^-)$ ). The  $\Delta\nu$  values ( $\Delta\nu = \nu_{\text{as}}(\text{COO}^-) - \nu_{\text{s}}(\text{COO}^-)$ ) [39,40]) were 62 and 146 cm<sup>-1</sup>, and indicated the formation of bidentate carboxylate complexes with chelated and bridged structures. The  $\nu(\text{C=O})$  vibrations for monodentate complexes could be located in the region of ~1600 cm<sup>-1</sup> [41], but the presence in this part of the spectrum of intense absorptions  $\nu(\text{CC})_{\text{ar}}$  and  $\nu(\text{C=C})$  did not allow for them to be detected.

The appearance of bands of pure *pCmA* in the spectra of *pCmA/CeO<sub>2</sub>* (0.6–1.2 mmol/g) samples was caused by the formation of *pCmA* associates on the oxide surface at concentrations close to or exceeding the value of the adsorption capacity [29].

Significant changes in the IR spectra of *pCmA/CeO<sub>2</sub>* samples, compared with pure acid, were found in the range of 1200–1400 cm<sup>-1</sup>. CH and COH vibrations [34,35] could appear here. From Figure 1, it was seen that in the spectra of *pCmA/CeO<sub>2</sub>* (0.1–0.6 mmol/g)

at  $1217\text{ cm}^{-1}$  the absorption of  $\beta(\text{CH})$  [35] disappeared. The  $1246\text{ cm}^{-1}$  ( $\beta(\text{OH})_{\text{ar}}$ –[35]) band for all  $p\text{CmA}/\text{CeO}_2$  samples was shifted to  $1250\text{ cm}^{-1}$ , and for concentrations  $0.1\text{--}0.6\text{ mmol/g}$  its intensity slightly decreased as compared to  $p\text{CmA}$ . Instead of a maximum at  $1284\text{ cm}^{-1}$  ( $\nu(\text{C-O})_{\text{ar}}$ –[35]), two peaks at  $1279$  and  $1290\text{ cm}^{-1}$  were detected for these samples. In addition, the intensity of the band at  $1315\text{ cm}^{-1}$  decreased, and the maximum of  $1329\text{ cm}^{-1}$  was absent. The origin of these bands was difficult to establish. In the study put forth by [35], the  $p\text{CmA}$  absorption in this region was attributed to  $\beta(\text{CH})_{\text{C=C}}$ . Although it was known that for phenolic acids (ferulic, vanilla, and caffeic),  $\beta(\text{OH})$  bands could also be found in this part of the spectrum [16,36–38,40]. The detected changes may have been due to the formation of carboxylate complexes on the oxide surface. At the same time, there were signs of phenolic group interaction with the  $\text{CeO}_2$  surface.

The interaction with the  $\text{CeO}_2$  surface also affected the other vibrations  $p\text{CmA}$  groups. In particular, for the  $p\text{CmA}/\text{CeO}_2$  ( $0.1\text{--}0.6\text{ mmol/g}$ ) samples, the maximum at  $1450\text{ cm}^{-1}$  ( $\nu(\text{CC})_{\text{ar}}$ –[35]) became invisible. Additionally, for all  $p\text{CmA}/\text{CeO}_2$  samples, there was a new peak at  $1440\text{ cm}^{-1}$ . It was known by [42] that carboxylate bands could occur in this area. The aromatic ring bands at  $1514$  and  $1603\text{ cm}^{-1}$  were shifted to the high-frequency region up to  $1516$  and  $1608\text{ cm}^{-1}$ , respectively. The  $\nu(\text{C=C})$  absorption at  $1628\text{ cm}^{-1}$  [35] was shifted to  $1633\text{ cm}^{-1}$ .

### 3.2. Pyrolysis of *p*-Coumaric Acid over Nanoceria

The results of the TPD MS study of  $p\text{CmA}/\text{CeO}_2$  samples were presented in Figures 2–5. Comparative analysis of the curve  $P = f(T)$  (Figure 2), mass spectra (Figure 3), and TPD curves for molecular and fragment ions of the main decomposition products (Figures 4 and 5) showed that the peak at  $\sim 150\text{ }^\circ\text{C}$  on the  $P/T$ -curve was due to the process decarboxylation. The thermal decomposition of  $p\text{CmA}$  on the  $\text{CeO}_2$  surface occurred in several stages from  $70$  to  $700\text{ }^\circ\text{C}$ . The maximum intensity of desorption gaseous products was registered at  $\sim 150\text{ }^\circ\text{C}$ .

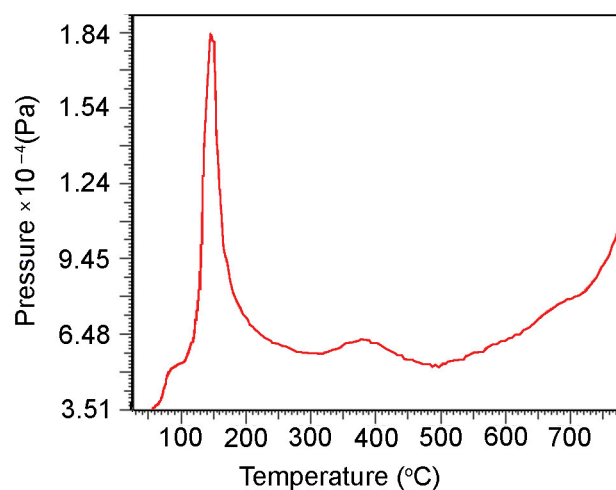


**Figure 2.** Vapor pressure of pyrolysis products measured as a function of temperature for the  $p\text{CmA}/\text{CeO}_2$  sample.

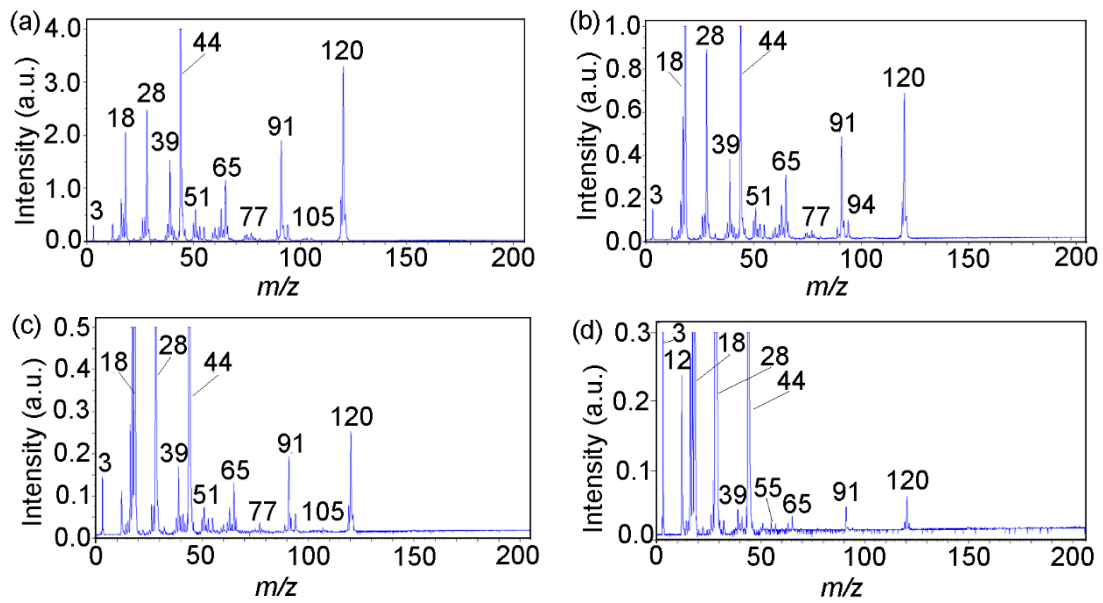


**Figure 3.** The mass spectra of *p*CmA/CeO<sub>2</sub> (0.6 mmol/g) obtained at temperatures of 120 °C (a), 250 °C (b), 350 °C (c), and 550 °C (d).

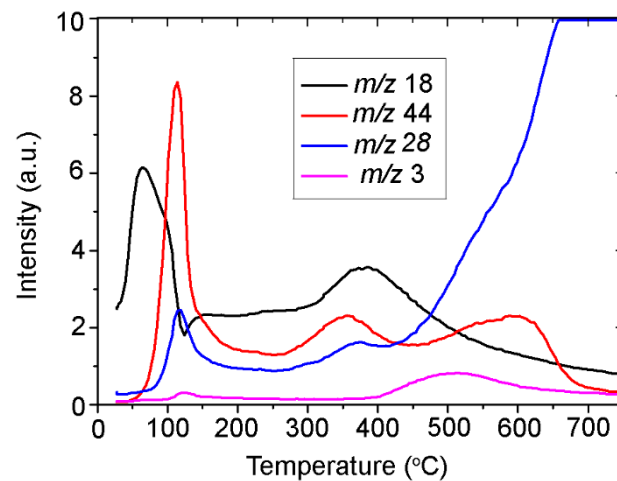


**Figure 4.** TPD curves for ions with *m/z* 3, 18, 28, and 44; obtained by decomposition of *p*CmA/CeO<sub>2</sub> (0.6 mmol/g).

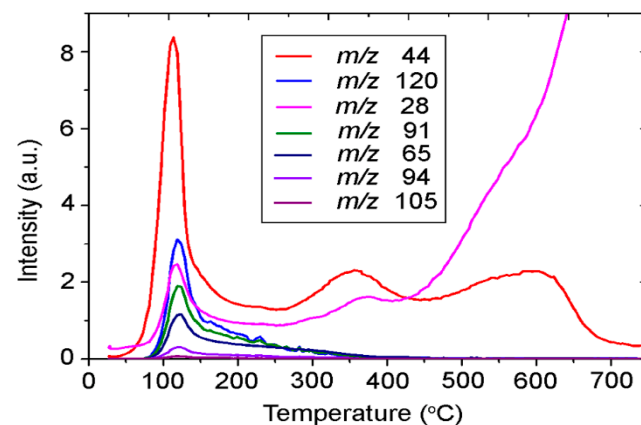


**Figure 5.** TPD curves for ions with *m/z* 28, 44, 65, 91, 94, 105, and 120; obtained by decomposition of *p*CmA/CeO<sub>2</sub> (0.6 mmol/g).

Earlier, we found that coumaric acid is a thermally unstable compound and decomposes via heating. Direct pyrolysis of coumaric acid proceeds as a decarboxylation reaction with the following kinetic parameters: temperature of the maximum desorption rate  $T_{max} = 115\text{ }^{\circ}\text{C}$ , reaction order  $n = 1$ , activation energy  $E^{\ddagger} = 79\text{ kJ/mol}$ , pre-exponential factor  $\nu_0 = 2.74 \times 10^8\text{ s}^{-1}$ , and activation entropy  $\Delta S^{\ddagger} = -20\text{ cal K}^{-1}\text{mol}^{-1}$  [11]. According to the calculated kinetic parameters [11], especially a negative value  $\Delta S^{\ddagger}$ , decarboxylation proceeds as an elimination reaction through a cyclic transition state.

The mass spectra of gaseous products of catalytic pyrolysis at 20–700  $^{\circ}\text{C}$  lacked the molecular ion of coumaric acid with  $m/z$  164 and its most characteristic fragment ions with  $m/z$  147, 119, 118, etc. (Figure 3). According to the standard database NIST Chemistry WebBook [43], in the electron ionization spectrum of *trans-p*-coumaric acid, the following ions were present:  $m/z$  164 (100%),  $m/z$  147 (~48%),  $m/z$  119 (~39%),  $m/z$  91 (~38%),  $m/z$  65 (~28%),  $m/z$  118 (~27%),  $m/z$  39 (~19%), and  $m/z$  107 (~15%).

Catalytic pyrolysis of coumaric acid also occurred due to decarboxylation with the release of  $\text{CO}_2$  ( $m/z$  44, 28) and 4-vinylphenol. The TPD curves of molecular and fragment ions of 4-vinyl phenol (M.r. = 120 Da,  $m/z$  120,  $m/z$  94 ( $\text{C}_6\text{H}_5\text{OH}$ ),  $m/z$  91 ( $\text{C}_7\text{H}_7$ )<sup>+</sup>,  $m/z$  77 ( $\text{C}_6\text{H}_5$ )<sup>+</sup>,  $m/z$  65 ( $\text{C}_5\text{H}_5$ )<sup>+</sup>,  $m/z$  39 ( $\text{C}_3\text{H}_3$ )<sup>+</sup>, and  $m/z$  105 ( $\text{C}_7\text{H}_4\text{OH}$ )<sup>+</sup>) repeated the shape of each other. However, this process on the surface of  $\text{CeO}_2$  proceeded in the broader temperature range of ~80–400  $^{\circ}\text{C}$ . In contrast, direct pyrolysis proceeded in the narrow range of ~80–160  $^{\circ}\text{C}$ .

The deconvolution of the TPD curve of 4-vinylphenol showed that this curve was likely a result of superposition of four TPD peaks at 118, 138, 184, and 262  $^{\circ}\text{C}$ , as shown in Figure 6. Moreover, the  $T_{max}$  of peak I and its localization (~80–150  $^{\circ}\text{C}$ ) were very close to those in the case of direct pyrolysis. Therefore, peak I was due to the decomposition of molecules, which was located on the surface, in the form of associates (Scheme 1). Their formation on the  $\text{CeO}_2$  surface was confirmed by the presence of absorptions in the IR spectra at  $1684\text{ cm}^{-1}$  and in the region of  $2400\text{--}2700\text{ cm}^{-1}$  (Figure 1, Table 2).

Analysis of our previous data of catalytic pyrolysis of cinnamic acids [16,40] and the results of deconvolution of the TPD curve for ion with  $m/z$  120 (4-vinylphenol) suggested that following peaks II–IV (Figure 6) were due to decarboxylation of different types of surface complexes (Scheme 2).

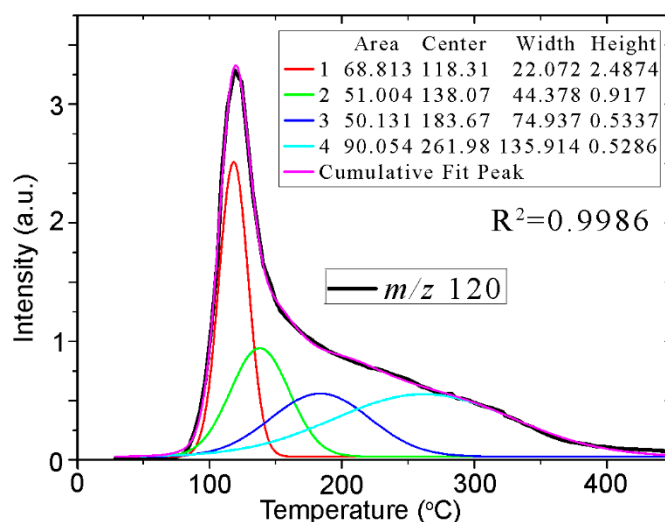
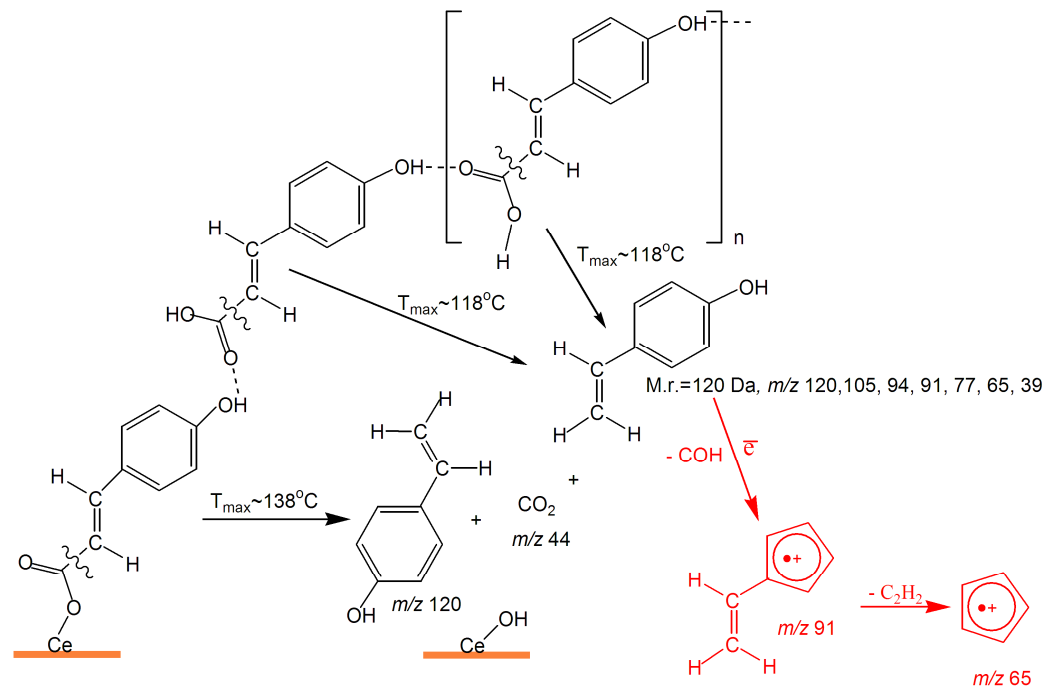
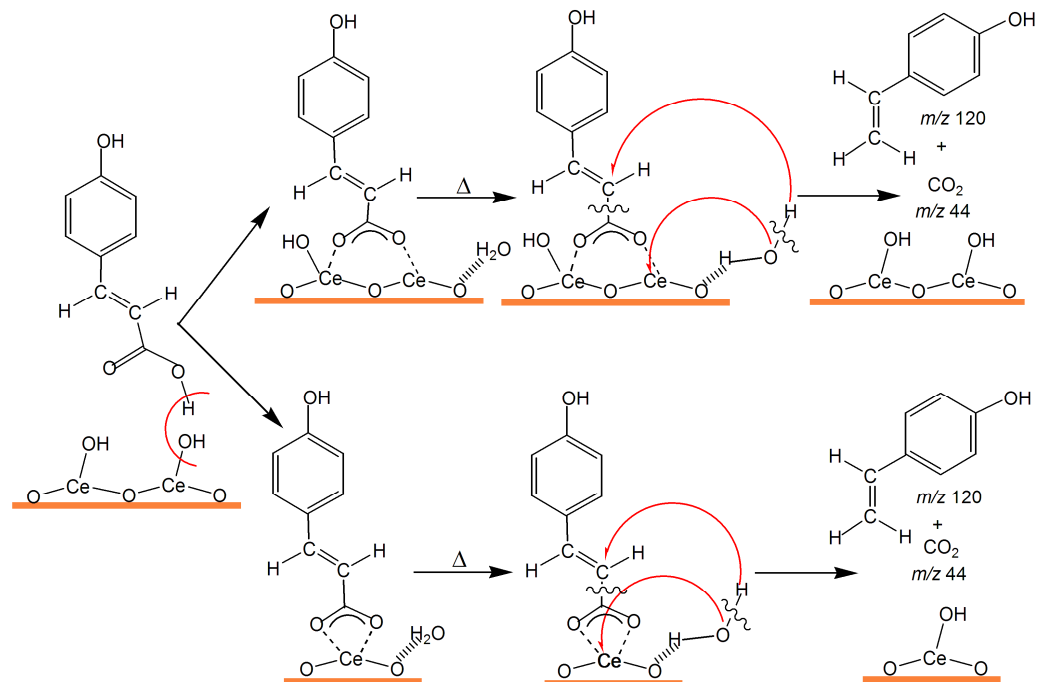


Figure 6. Deconvolution of TPD curve for ion with  $m/z$  120 (4-vinylphenol).



**Scheme 1.** Decarboxylation of monodentate bounded complexes and associates of coumaric acid on the nanoceria surface with release of 4-vinylphenol.



**Scheme 2.** Decarboxylation of bidentate bridging and bidentate chelate carboxylate complexes of coumaric acid.

Peaks II, III, and IV were likely due to decarboxylation of monodentate, bidentate bridging, and bidentate chelate carboxylate complexes, respectively (Schemes 1 and 2). The presence of these complexes was confirmed by IR spectroscopy data (Figure 1 and Table 2). Although the decomposition products of these complexes were the same (4-vinylphenol and  $\text{CO}_2$ ), the temperatures of the maximum desorption rate of these products differed. This fact was due to the strength of the complexes formed. The more strongly the complex

was bound to the surface, the higher the temperature of its decomposition and, accordingly, the activation energy of the decarboxylation reaction.

It is known that the strength of carboxylate complexes increases in the following order: monodentate < bidentate bridging < bidentate chelate. The temperature of the peak maximum  $T_{max}$  was usually used for semi-quantitative estimates of the activation energies of reactions [25,26,30,44–46]. We used the modified Equation (1) suggested by Kislyuk and Rozanov based on the Redhead equation [44,45]:

$$E^\ddagger = R T_{max} \ln(B/\ln B) \quad (1)$$

$$B = (n\nu_0 T_{max} C_{max}^{n-1})b \quad (2)$$

where  $n$  is the reaction order,  $\nu_0$  is the pre-exponential factor,  $C_{max}^{n-1}$  is the concentration of the adsorbate at  $T_{max}$ , and  $b$  is the value of the sample heating rate. The activation energies for decarboxylation of surface complexes of coumaric acid were calculated using Equation (1) and on the assumption that the reaction order and the pre-exponential factor for decarboxylation of these complexes were equal to the same as for the condensed state ( $n = 1$ ,  $\nu_0 = 10^8$  s) (Table 3). Due to the deconvolution of the TPD curve of the molecular ion of 4-vinylphenol (Figure 6), it was possible to roughly estimate the relative amount of surface complexes (Table 3). It resulted that the largest amount of the most stable chelate complexes were formed, at about 35%.

**Table 3.** The calculated integral intensities for the peaks of molecular ions of 4-vinylphenol with  $m/z = 120$ ; the relative amount of coumaric surface complexes.

Nº	Surface Complexes (SC)	$m/z$	$T_{max}$ (°C)	<sup>a</sup> $E^\ddagger$ , kJ·mol <sup>-1</sup>	Scheme	Peak Area (a.u.)	%
I	H-bonded associates	120	118	80	1	69	27
II	Monodentate bonded complexes	120	138	84	1	51	19
III	Bidentate bridging carboxylates	120	184	93	2	50	19
IV	Bidentate chelate carboxylates	120	262	109	2	90	35

$$^a E^\ddagger = R T_{max} \ln(B/\ln B), n = 1, \nu_0 = 10^8 \text{ s.}$$

No transformations could be clearly associated with the decomposition of phenolate complexes, in contrast to other carboxylic acids (caffeic, ferulic, and vanillic) on the CeO<sub>2</sub> surface [16,40]. In the presence of one OH group in the *para*-position of the aromatic ring, the interaction of carboxylic acids with the CeO<sub>2</sub> surface through the carboxyl group could likely be energetically more favorable

### 3.3. Thermogravimetric Analysis

According to TGA/DTG/DTA data (Figure 7 and Table 4), the decomposition of the *p*CmA/CeO<sub>2</sub> sample occurred in the temperature range of 70 to 500 °C in four stages. All stages were exothermic. Comparing the DTG (Figure 7) and TPD MS (Figure 6) data, it was found that the number of *p*CmA/CeO<sub>2</sub> degradation steps were the same.

**Table 4.** Thermolysis yields obtained during thermogravimetric analysis of the sample of *p*CmA /CeO<sub>2</sub> (0.6 mmol/g).

Sample	Stage	$T_{max}$ (°C)	Weight Loss (%)
<i>p</i> CmA/CeO <sub>2</sub>	I	90	4
	II	153	16
	III	255	33
	IV	288	47

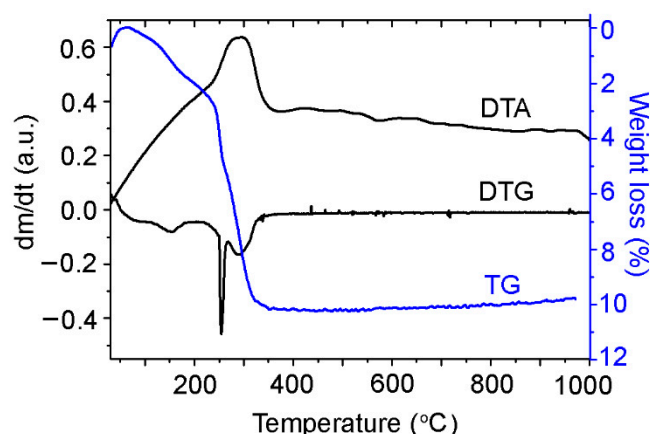


**Figure 7.** Differential thermal analysis (DTA), differential thermogravimetric analysis (DTG), and thermogravimetric (TG) curves for *pCmA/CeO<sub>2</sub>* (0.6 mmol/g).

The most significant weight loss corresponding to the fourth stage (~290 °C) occurred mainly due to the decomposition of carboxylates with a chelating bidentate type of coordination (Table 4). This fact was in complete agreement with the data of a semi-quantitative assessment of the relative amount of these complexes, and the activation energy of their decomposition, according to TPD MS data (Table 3).

#### 4. Conclusions

In the study of *pCmA* on the nanoceria surface by FT-IR spectroscopy and TPD MS, it was found that the *pCmA* interaction with oxide occurred mainly through the participation of the carboxyl group. Carboxylate complexes, formed on the nanoceria surface, were monodentate and bidentate with bridge and chelate structures. Their thermal destruction occurred by decarboxylation. The obtained data could help study and control the mechanisms of pyrolytic transformations of lignin-containing raw materials using catalysts containing cerium dioxide.

**Author Contributions:** Conceptualization, T.K., M.K. and M.L.; methodology, T.K., N.N. and B.P.; investigation, N.N., B.P., T.K. and T.C.; resources, T.K.; writing—original draft preparation, N.N. and T.K.; writing—review and editing, T.K., N.N. and M.L.; visualization, N.N., T.K. and B.P.; supervision, T.K., M.K. and M.L.; project administration, T.K.; funding acquisition, T.K. and M.L. All authors have read and agreed to the published version of the manuscript.

**Funding:** This publication is based on work supported by the grant FSA3-20-66700 from the U.S. Civilian Research and Development Foundation (CRDF Global) with funding from the United States Department of State, by the Swedish Research Council (VR) under contract 348-2014-4250, and by NAS of Ukraine (Program “New functional substances and materials of chemical production”).

**Institutional Review Board Statement:** Not applicable.

**Informed Consent Statement:** Not applicable.

**Data Availability Statement:** The study did not report any data.

**Conflicts of Interest:** The authors declare no conflict of interest.

#### References

1. Kiliç, I.; Yeşiloğlu, Y. Spectroscopic studies on the antioxidant activity of *p*-coumaric acid. *Spectrochim. Acta Part A Mol. Biomol. Spectrosc.* **2013**, *115*, 719–724. [[CrossRef](#)] [[PubMed](#)]
2. Pei, K.; Ou, J.; Huang, J.; Ou, S. *p*-Coumaric acid and its conjugates: Dietary sources, pharmacokinetic properties and biological activities. *J. Sci. Food Agric.* **2016**, *96*, 2952–2962. [[CrossRef](#)]
3. Saha, K.; Dasgupta, J.; Chakraborty, S.; Antunes, F.A.F.; Sikder, J.; Curcio, S.; dos Santos, J.C.; Arafat, H.A.; da Silva, S.S. Optimization of lignin recovery from sugarcane bagasse using ionic liquid aided pretreatment. *Cellulose* **2017**, *24*, 3191–3207. [[CrossRef](#)]

4. Karlen, S.D.; Fasahati, P.; Mazaheri, M.; Serate, J.; Smith, R.A.; Sirobhusanam, S.; Chen, M.; Tymokhin, V.I.; Cass, C.L.; Liu, S.; et al. Assessing the viability of recovery of hydroxycinnamic acids from lignocellulosic biorefinery alkaline pretreatment waste streams. *ChemSusChem* **2020**, *13*, 2012–2024. [[CrossRef](#)]
5. Dhyani, V.; Bhaskar, T. Pyrolysis of biomass. In *Biofuels: Alternative Feedstocks and Conversion Processes for the Production of Liquid and Gaseous Biofuels*; Academic Press: Cambridge, MA, USA, 2019; pp. 217–244. [[CrossRef](#)]
6. Ralph, J.; Hatfield, R.D.; Quideau, S.; Helm, R.F.; Grabber, J.H.; Jung, H.J.G. Pathway of p-coumaric acid incorporation into maize lignin as revealed by NMR. *J. Am. Chem. Soc.* **1994**, *116*, 9448–9456. [[CrossRef](#)]
7. Jose, C.; Gutiérrez, A.; Rodríguez, I.M.; Ibarra, D.; Martínez, A.T. Composition of non-woody plant lignins and cinnamic acids by Py-GC/MS, Py/TMAH and FT-IR. *J. Anal. Appl. Pyrolysis* **2007**, *79*, 39–46. [[CrossRef](#)]
8. Van der Hage, E.R.; Mulder, M.M.; Boon, J.J. Structural characterization of lignin polymers by temperature-resolved in-source pyrolysis—mass spectrometry and Curie-point pyrolysis—Gas chromatography/mass spectrometry. *J. Anal. Appl. Pyrolysis* **1993**, *25*, 149–183. [[CrossRef](#)]
9. Chakar, F.S.; Ragauskas, A.J. Review of current and future softwood kraft lignin process chemistry. *Ind. Crops Prod.* **2004**, *20*, 131–141. [[CrossRef](#)]
10. Zakzeski, J.; Bruijninx, P.C.; Jongerius, A.L.; Weckhuysen, B.M. The catalytic valorization of lignin for the production of renewable chemicals. *Chem. Rev.* **2010**, *110*, 3552–3599. [[CrossRef](#)]
11. Kulik, T.; Barvinchenko, V.N.; Palyanytsya, B.B.; Lipkovska, N.A.; Dudik, O.O. Thermal transformations of biologically active derivatives of cinnamic acid by TPD MS investigation. *J. Anal. Appl. Pyrolysis* **2011**, *90*, 219–223. [[CrossRef](#)]
12. Hartley, R.D.; Haverkamp, J. Pyrolysis-mass spectrometry of the phenolic constituents of plant cell walls. *J. Sci. Food Agric.* **1984**, *35*, 14–20. [[CrossRef](#)]
13. Mulder, M.M.; Van Der Hage, E.R.; Boon, J.J. Analytical in source pyrolytic methylation electron impact mass spectrometry of phenolic acids in biological matrices. *Phytochem. Anal.* **1992**, *3*, 165–172. [[CrossRef](#)]
14. Dijkstra, E.F.; Boon, J.J.; Van Mourik, J.M. Analytical pyrolysis of a soil profile under Scots pine. *Europ. J. Soil Sci.* **1998**, *49*, 295–304. [[CrossRef](#)]
15. Trovarelli, A. Catalytic properties of ceria and CeO<sub>2</sub>-containing materials. *Catal. Rev.* **1996**, *38*, 439–520. [[CrossRef](#)]
16. Nastasiienko, N.; Kulik, T.; Palianytsia, B.; Laskin, J.; Cherniavska, T.; Kartel, M.; Larsson, M. Catalytic Pyrolysis of Lignin Model Compounds (Pyrocatechol, Guaiacol, Vanillic and Ferulic Acids) over Nanoceria Catalyst for Biomass Conversion. *Appl. Sci.* **2021**, *11*, 7205. [[CrossRef](#)]
17. Deng, W.; Zhang, H.; Wu, X.; Li, R.; Zhang, Q.; Wang, Y. Oxidative conversion of lignin and lignin model compounds catalyzed by CeO<sub>2</sub>-supported Pd nanoparticles. *Green Chem.* **2015**, *17*, 5009–5018. [[CrossRef](#)]
18. Schimming, S.M.; LaMont, O.D.; König, M.; Rogers, A.K.; D’Amico, A.D.; Yung, M.M.; Sievers, C. Hydrodeoxygenation of guaiacol over ceria–zirconia catalysts. *ChemSusChem* **2015**, *8*, 2073–2083. [[CrossRef](#)]
19. Song, W.L.; Dong, Q.; Hong, L.; Tian, Z.Q.; Tang, L.N.; Hao, W.; Zhang, H. Activating molecular oxygen with Au/CeO<sub>2</sub> for the conversion of lignin model compounds and organosolv lignin. *RSC Adv.* **2019**, *9*, 31070–31077. [[CrossRef](#)]
20. Totong, S.; Daorattanachai, P.; Laosiripojana, N.; Idem, R. Catalytic depolymerization of alkaline lignin to value-added phenolic-based compounds over Ni/CeO<sub>2</sub>-ZrO<sub>2</sub> catalyst synthesized with a one-step chemical reduction of Ni species using NaBH<sub>4</sub> as the reducing agent. *Fuel Process. Technol.* **2020**, *198*, 106248. [[CrossRef](#)]
21. Gliński, M.; Kijeński, J.; Jakubowski, A. Ketones from monocarboxylic acids: Catalytic ketonization over oxide systems. *Appl. Catal. A Gen.* **1995**, *128*, 209–217. [[CrossRef](#)]
22. Deng, L.; Fu, Y.; Guo, Q.X. Upgraded acidic components of bio-oil through catalytic ketonic condensation. *Energy Fuels* **2008**, *23*, 564–568. [[CrossRef](#)]
23. Vlasenko, N.V.; Kyriienko, P.I.; Yanushevska, O.I.; Valihura, K.V.; Soloviev, S.O.; Strizhak, P.E. The Effect of Ceria Content on the Acid–Base and Catalytic Characteristics of ZrO<sub>2</sub>–CeO<sub>2</sub> Oxide Compositions in the Process of Ethanol to n-Butanol Condensation. *Catal. Lett.* **2020**, *150*, 234–242. [[CrossRef](#)]
24. Sharanda, L.F.; Shimansky, A.P.; Kulik, T.V.; Chuiko, A.A. Study of acid-base surface properties of pyrogenic  $\gamma$ -aluminium oxide. *Colloids Surf. A* **1995**, *105*, 167–172. [[CrossRef](#)]
25. Kulik, T.; Palianytsia, B.; Larsson, M. Catalytic Pyrolysis of Aliphatic Carboxylic Acids into Symmetric Ketones over Ceria-Based Catalysts: Kinetics, Isotope Effect and Mechanism. *Catalysts* **2020**, *10*, 179. [[CrossRef](#)]
26. Kulyk, K.; Palianytsia, B.; Alexander, J.D.; Azizova, L.; Borysenko, M.; Kartel, M.; Larsson, M.; Kulik, T. Kinetics of valeric acid ketonization and ketenization in catalytic pyrolysis on nanosized SiO<sub>2</sub>,  $\gamma$ -Al<sub>2</sub>O<sub>3</sub>, CeO<sub>2</sub>/SiO<sub>2</sub>, Al<sub>2</sub>O<sub>3</sub>/SiO<sub>2</sub> and TiO<sub>2</sub>/SiO<sub>2</sub>. *ChemPhysChem* **2017**, *18*, 1943–1955. [[CrossRef](#)]
27. Kanimozhi, C.; Kim, M.; Larson, S.R.; Choi, J.W.; Choo, Y.; Sweat, D.P.; Osuji, C.O.; Gopalan, P. Isomeric Effect Enabled Thermally Driven Self-Assembly of Hydroxystyrene-Based Block Copolymers. *ACS Macro Lett.* **2016**, *5*, 833–838. [[CrossRef](#)]
28. Matuszewska, A.; Uchman, M.; Adamczyk-Woźniak, A.; Sporzyński, A.; Pispas, S.; Kováčik, L.; Štěpánek, M. Glucose-Responsive Hybrid Nanoassemblies in Aqueous Solutions: Ordered Phenylboronic Acid within Intermixed Poly(4-hydroxystyrene)-block-poly(ethylene oxide) Block Copolymer. *Biomacromolecules* **2015**, *16*, 3731–3739. [[CrossRef](#)]
29. Barvinchenko, V.N.; Lipkovskaya, N.A.; Kulik, T.V. Adsorption of Natural 3-Phenylpropenic Acids on Cerium Dioxide Surface. *Colloid J.* **2019**, *81*, 1–7. [[CrossRef](#)]

30. Kulyk, K.; Ishchenko, V.; Palyanytsya, B.; Khylyla, V.; Borysenko, M.; Kulyk, T. A TPD-MS study of the interaction of coumarins and their heterocyclic derivatives with a surface of fumed silica and nanosized oxides CeO<sub>2</sub>/SiO<sub>2</sub>, TiO<sub>2</sub>/SiO<sub>2</sub>, Al<sub>2</sub>O<sub>3</sub>/SiO<sub>2</sub>. *J. Mass Spectrom.* **2010**, *45*, 750–761. [CrossRef]
31. Kulyk, K.; Zettergren, H.; Gatchell, M.; Alexander, J.D.; Larsson, M.; Borysenko, M.; Palianytsia, B.; Kulik, T. Dimethylsilanone Generation from Pyrolysis of Polysiloxanes Filled with Nanosized Silica and Ceria/Silica. *ChemPlusChem* **2016**, *81*, 1003–1013. [CrossRef]
32. Kulyk, K.; Borysenko, M.; Kulik, T.; Mikhalovska, L.; Alexander, J.D.; Palianytsia, B. Chemisorption and thermally induced transformations of polydimethylsiloxane on the surface of nanoscale silica and ceria/silica. *Polym. Degrad. Stab.* **2015**, *120*, 203–211. [CrossRef]
33. Kulik, T.V.; Lipkovska, N.O.; Barvinchenko, V.M.; Palyanytsya, B.B.; Kazakova, O.A.; Dudik, O.O.; Menyhárd, A.; László, K. Thermal transformation of bioactive caffeic acid on fumed silica seen by UV–Vis spectroscopy, thermogravimetric analysis, temperature programmed desorption mass spectrometry and quantum chemical methods. *J. Colloid Interface Sci.* **2016**, *470*, 132–141. [CrossRef]
34. Bellamy, L. *Infra-Red Spectra of Complex Molecule*; Methuen & Co. Ltd.: London, UK, 1963.
35. Świsłocka, R.; Kowczyk-Sadowy, M.; Kalinowska, M.; Lewandowski, W. Spectroscopic (FT-IR, FT-Raman, <sup>1</sup>H and <sup>13</sup>C NMR) and theoretical studies of p-coumaric acid and alkali metal p-coumarates. *Spectroscopy* **2012**, *27*, 35–48. [CrossRef]
36. Sebastian, S.; Sundaraganesan, N.; Manoharan, S. Molecular structure, spectroscopic studies and first-order molecular hyperpolarizabilities of ferulic acid by density functional study. *Spectrochim. Acta Part A Mol. Biomol. Spectrosc.* **2009**, *74*, 312–323. [CrossRef]
37. González-Baró, A.C.; Parajón-Costa, B.S.; Franca, C.A.; Pis-Diez, R. Theoretical and spectroscopic study of vanillic acid. *J. Molec. Struct.* **2008**, *889*, 204–210. [CrossRef]
38. Świsłocka, R. Spectroscopic (FT-IR, FT-Raman, UV absorption, <sup>1</sup>H and <sup>13</sup>C NMR) and theoretical (in B3LYP/6-311++ G\*\* level) studies on alkali metal salts of caffeic acid. *Spectrochim. Acta Part A Mol. Biomol. Spectrosc.* **2013**, *100*, 21–30. [CrossRef] [PubMed]
39. Palacios, E.G.; Juárez-López, G.; Monhemius, A.J. Infrared spectroscopy of metal carboxylates: II. Analysis of Fe (III), Ni and Zn carboxylate solutions. *Hydrometallurgy* **2004**, *72*, 139–148. [CrossRef]
40. Nastasiienko, N.; Palianytsia, B.; Kartel, M.; Larsson, M.; Kulik, T. Thermal Transformation of Caffeic Acid on the Nanoceria Surface Studied by Temperature Programmed Desorption Mass-Spectrometry, Thermogravimetric Analysis and FT-IR Spectroscopy. *Colloids Interfaces* **2019**, *3*, 34. [CrossRef]
41. Ding, S.; Zhao, J.; Yu, Q. Effect of Zirconia Polymorph on Vapor-Phase Ketonization of Propionic Acid. *Catalysts* **2019**, *9*, 768–773. [CrossRef]
42. Van Den Brand, J.; Blajiev, O.; Beentjes, P.C.J.; Terryn, H.; De Wit, J.H.W. Interaction of anhydride and carboxylic acid compounds with aluminum oxide surfaces studied using infrared reflection absorption spectroscopy. *Langmuir* **2004**, *20*, 6308–6317. [CrossRef]
43. Stein, S.E. *NIST Chemistry WebBook*; Mallard, W.G., Linstrom, P.J., Eds.; National Institute of Standards and Technology: Gaithersburg, MD, USA, 2000. Available online: <http://webbook.nist.gov> (accessed on 14 October 2021).
44. Redhead, P.A. Thermal Desorption of Gases. *Vacuum* **1962**, *12*, 203–211. [CrossRef]
45. Kislyuk, M.U.; Rozanov, V.V. Temperature-programmed desorption and temperature-programmed reaction—methods of studying of kinetics and mechanisms of catalytic processes. *Kinet. Catal.* **1995**, *36*, 89–98.
46. Kulik, T.V. Use of TPD-MS and linear free energy relationships for assessing the reactivity of aliphatic carboxylic acids on a silica surface. *J. Phys. Chem. C* **2012**, *116*, 570–580. [CrossRef]